Supporting Information

Engineering Functionality in Organic Porous Networks by Multicomponent Polymerization

Bingyan Zhou,[†] *Zixu Chen,[†] Shengyu Feng, [†‡] Dengxu Wang,*[†‡] Hongzhi Liu*[†]

[†] National Engineering Research Center for Colloidal Materials & Key Laboratory of Special Functional Aggregated Materials, Ministry of Education, School of Chemistry and Chemical Engineering, Shandong University, Jinan 250100, P. R. China

[‡] Shandong Key Laboratory of Advanced Organosilicon Materials and Technologies & State Key Laboratory of Fluorinated Functional Membrane Materials, Zibo 256401, P. R. China

*Corresponding author's e-mail: dxwang@sdu.edu.cn

Table of contents

Table S2. EDS analysis data for CPOP and AIPOP-1 to AIPOP-4

Table S3. Porosity data of CPOP and AIPOP-1 to AIPOP-4

Table S4. Kinetic parameters for the adsorption of I_2 by AIPOP-4

Table S5. Kinetic parameters for the adsorption of iodine solution by AIPOP-4

Table S6. Summary of the Langmuir and Freundlich isotherm model parameters for the adsorption of iodine solution by AIPOP-4

Table S7. Electronic binding energy of various elements in iodine-loaded CPOP and AIPOP-4

Characterization. Fourier transform infrared (FT-IR) spectra were measured within a 4000 to 400 cm^{-1} region on a Bruker TENSOR-27 infrared spectrophotometer (KBr pellet). ^{1}H NMR, ^{13}C NMR and ^{29}Si NMR spectra were measured on a Bruker AVANCE-300 or 400 NMR spectrometer. Solid-state ^{13}C cross-polarization/magic-angle-spinning (CP/MAS) NMR data was collected on Bruker AVANCE-500 NMR Spectrometer operating at a magnetic field strength of 9.4 T. The resonance frequencies at this field strength were 125 MHz for ^{13}C NMR respectively. A chemagnetics 5 mm triple- resonance MAS probe was used to acquire ^{13}C NMR spectra. Elemental analyses were measured using an Elementar Vario EL III elemental analyzer and Oxford INCA X-sight energy dispersive X-ray spectrometry.

Thermogravimetric analysis (TGA) was conducted under N_2 using a TA SDTQ600 at a temperature range of room temperature to 800°C with a heating rate of 10 °C min^{-1}. Field-emission scanning electron microscopy (FE-SEM) experiments were determined by using HITACHI S4800 Spectrometer. Powder X-ray diffraction (PXRD) were carried out on a Riguku D/MAX 2550 diffractometer with Cu-Kα radiation, 40 kV, 20 mA with the 2θ range of 10°~90° (scanning rate of 10° min^{-1}) at

room temperature. Nitrogen sorption isotherm measurements were performed using a Micro meristics surface area and a pore size analyzer. Before measurement, the samples were degassed at 100°C for at least 12 h. A sample of ca. 100 mg and a UHP-grade nitrogen (99.999%) gas source were used for the nitrogen sorption measurements conducted at 77K and collected on a Quantachrome Quadrasorb apparatus. Brunauer-Emmett-Teller (BET) surface areas were determined over a P/P_0 range from 0.01 to 0.20. Nonlocal density functional theory (NLDFT) pore size distributions were determined using the carbon/slit cylindrical pore mode of the Quadrawin software. X-ray photoelectron spectroscopy (XPS) was conducted on a Thermo Fischer ESCALAB 250Xi using a monochromatic Al Kα (1486.8 eV) X-ray source with a spot size of 500 μm. The anode was operated at 12.5 kV and 16 mA. Raman spectra were collected by using a micro-Raman LabRAM HR800 spectrometer (Horiba Jobin Yvon, Japan) equipped with a 633 nm laser as an excitation source. Ultraviolet absorption (UV) spectra were performed with TU-1901 double UV–Vis spectrophotometer.

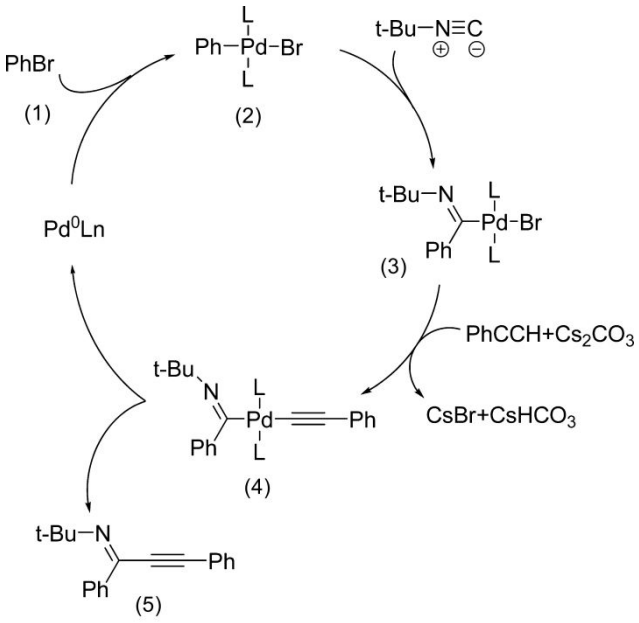

Scheme S1. Plausible mechanism of the Pd-catalyzed multicomponent reaction of bromoarenes, isonitriles and alkynes

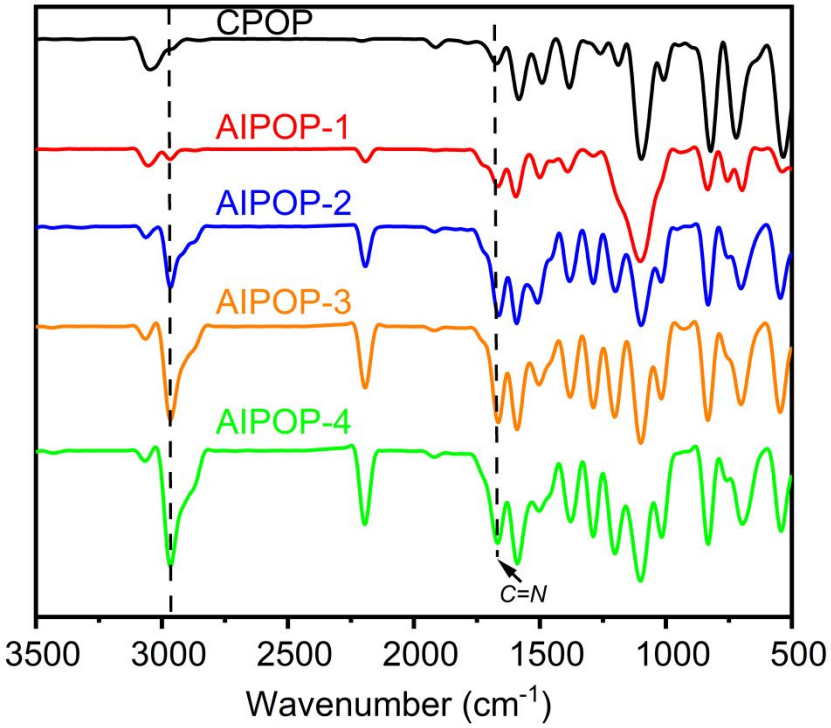

Figure S1. FT-IR spectroscopy of CPOP and AIPOP-1 to AIPOP-4. The peaks at 1665 cm^{-1} in AIPOPs are assigned to both C=C and C=N stretching vibrations, while this peak in CPOP belongs to the C=C stretching vibration. This assignment could be evidenced by the gradually enhanced absorption intensities of C=N peaks with an increment of imine contents in AIPOPs.

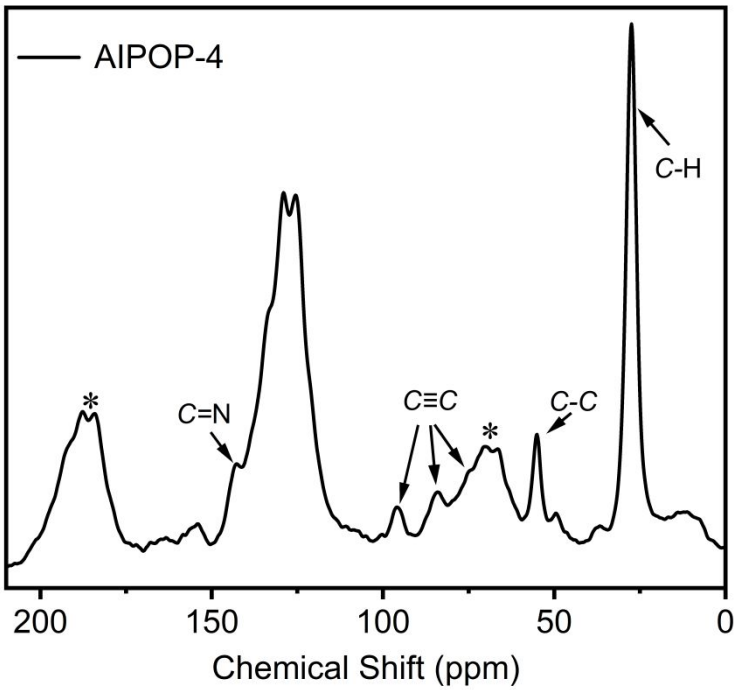

Figure S2. ^{13}C NMR spectra of AIPOP-4 in the solid-state. Asterisks denote the spinning sidebands.

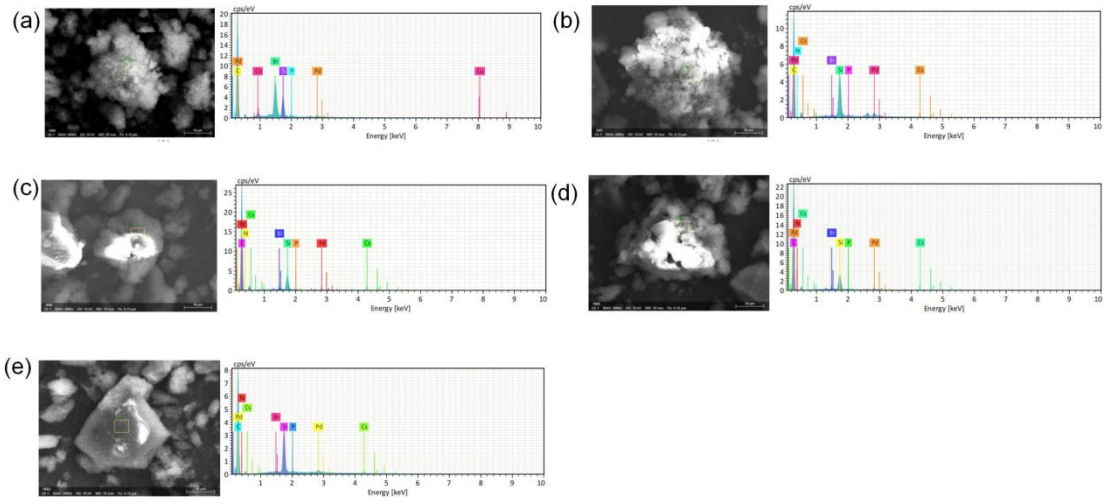

Figure S3. Energy dispersive spectroscopy of CPOP (a) and AIPOP-1 to AIPOP-4 (b-e)

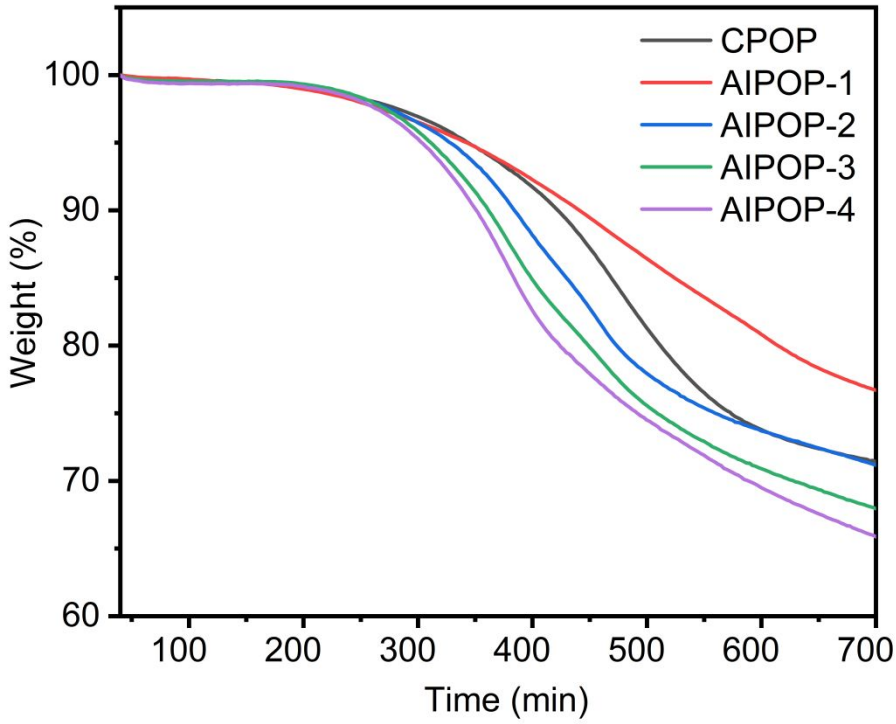

Figure S4. TGA curve of CPOP and AIPOP-1~AIPOP-4 under N_2 atmosphere with a heating rate of 10°C min^{-1}

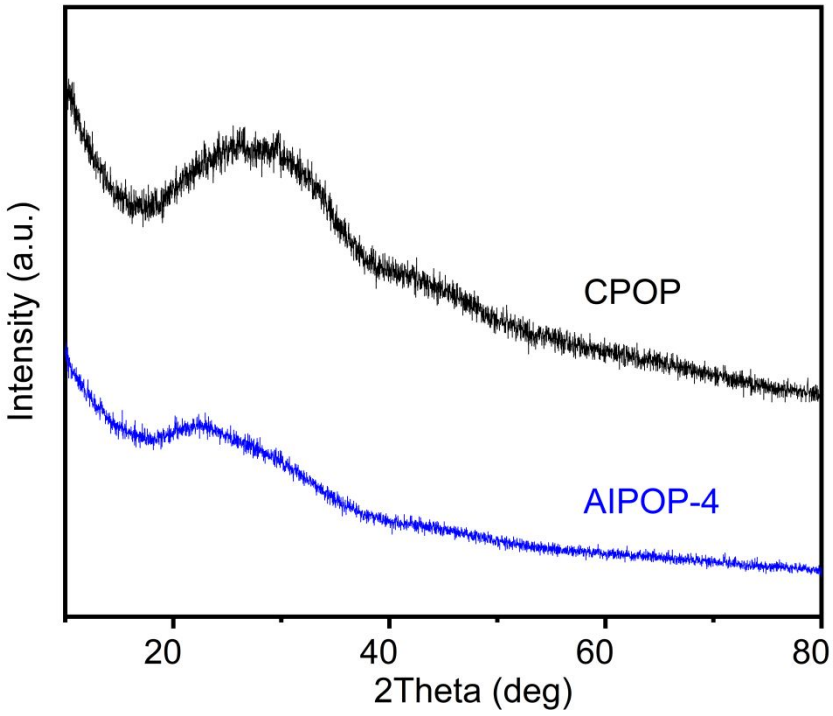

Figure S5. XRD spectra of CPOP and AIPOP-4.

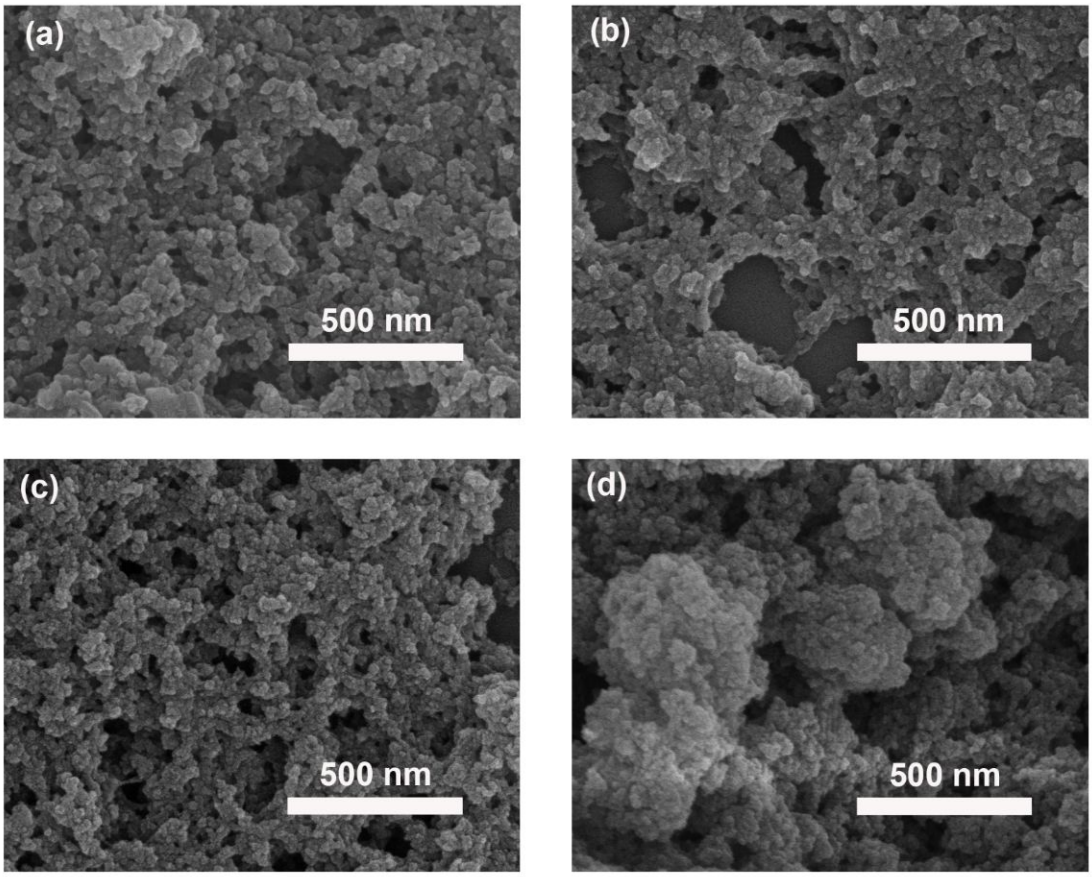

Figure S6. SEM images of AIPOP-4 (a), AIPOP-3 (b), AIPOP-2 (c), and AIPOP-1 (d)

Figure S7. Colour change of AIPOP-4 after the iodine adsorption

Figure S8. Photographs of iodine desorption process of CPOP (a), AIPOP-1 (b), AIPOP-2 (c), AIPOP-3 (d), and AIPOP-4 (e) in ethanol from 5 min to 24 h. The same weight iodine loaded samples (20 mg) were immersed in ethanol (4 mL) at room temperature

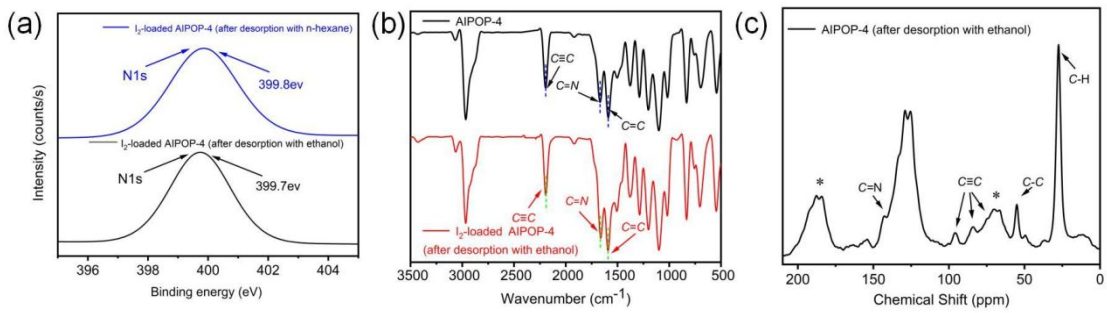

Figure S9. (a) High-resolution XPS spectra of N1s for AIPOP-4 and iodine-loaded AIPOP-4 after desorption with ethanol and *n*-hexane; (b) FT-IR spectra of AIPOP-4 and iodine-loaded AIPOP-4 after desorption with ethanol; (c) ^{13}C NMR spectra of iodine-loaded AIPOP-4 after desorption with ethanol.

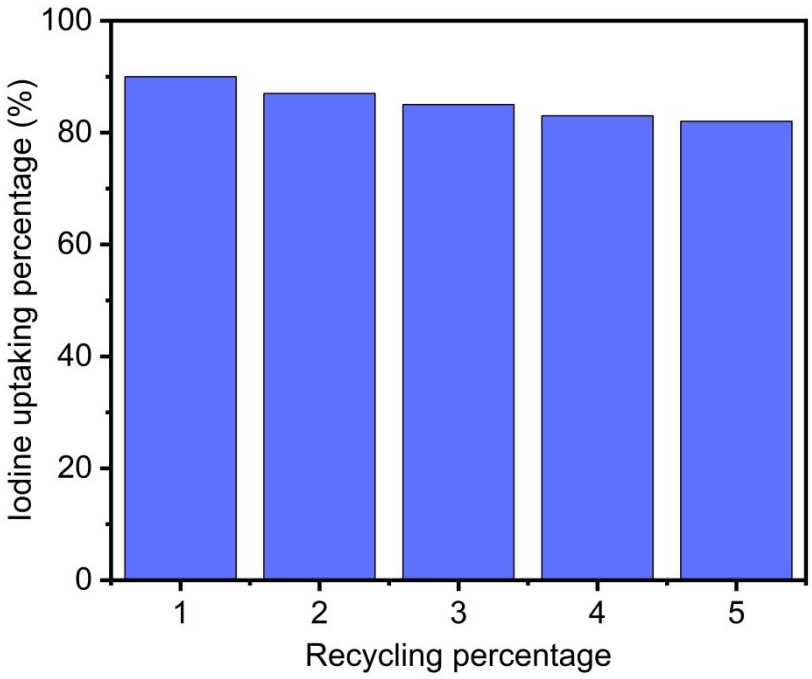

Figure S10. Recyclability of AIPOP-4 (after desorption with n-hexane) for I_2 capture

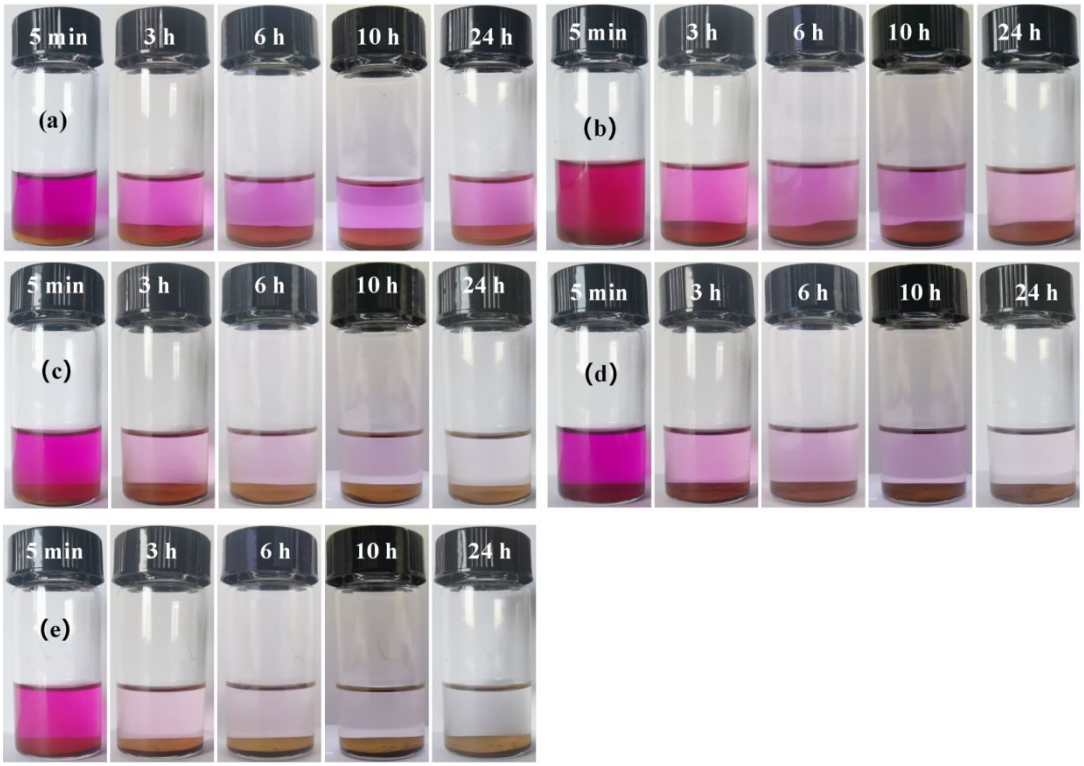

Figure S11. Photographs of iodine capture in n-hexane solutions by CPOP (a), AIPOP-1 (b), AIPOP-2 (c), AIPOP-3 (d), and AIPOP-4 (e) from 5 min to 24 h. The same weight CPPs (20 mg) were immersed in iodine solutions (c = 6 mM, 5 mL) at 25 ℃.

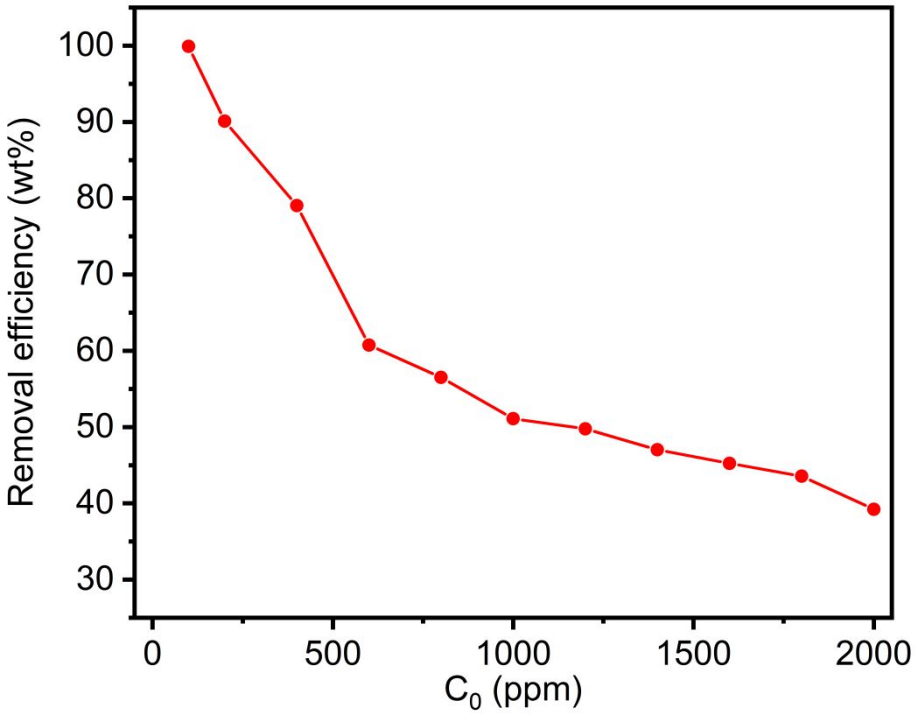

Figure S12. The effect of the initial iodine concentrations on the removal efficiency by AIPOP-4 (1 mg/mL)

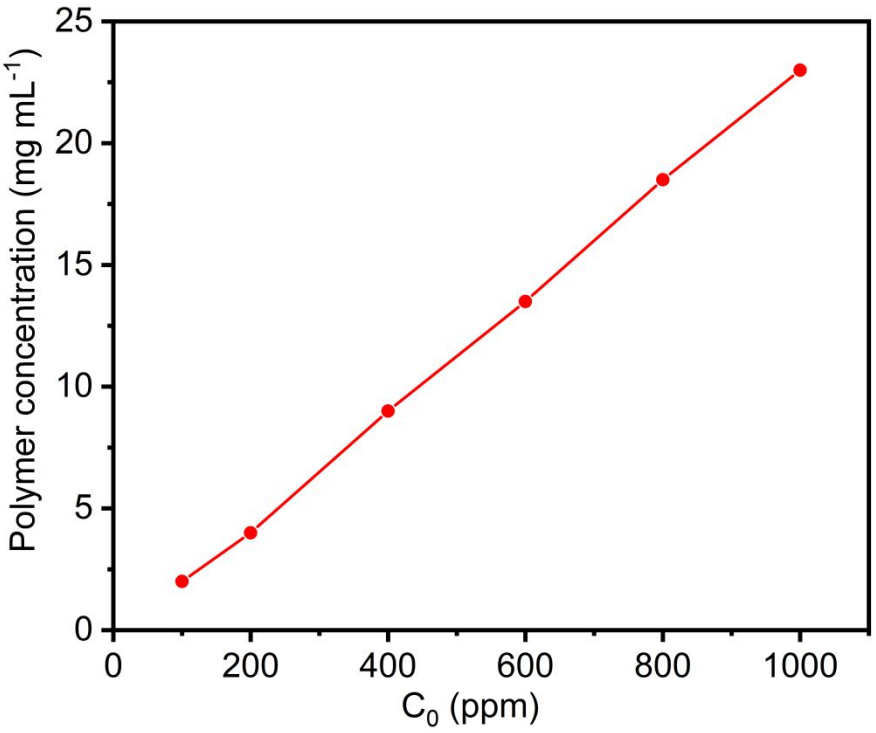

Figure S13. Mass of AIPOP-4 required for complete removal of iodine in different concentrations

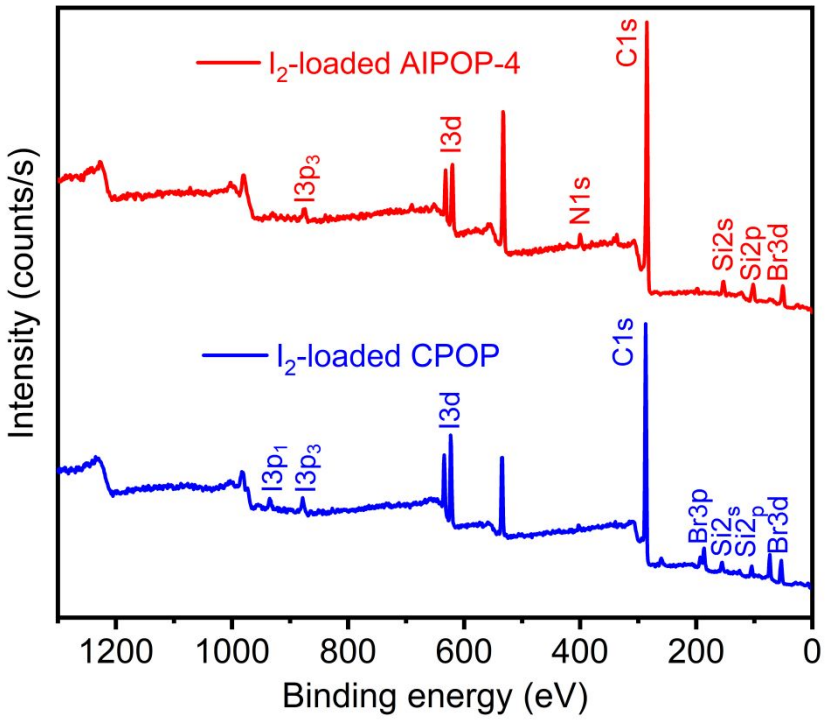

Figure S14. Wide-scan XPS spectra of iodine-loaded CPOP and AIPOP-4;

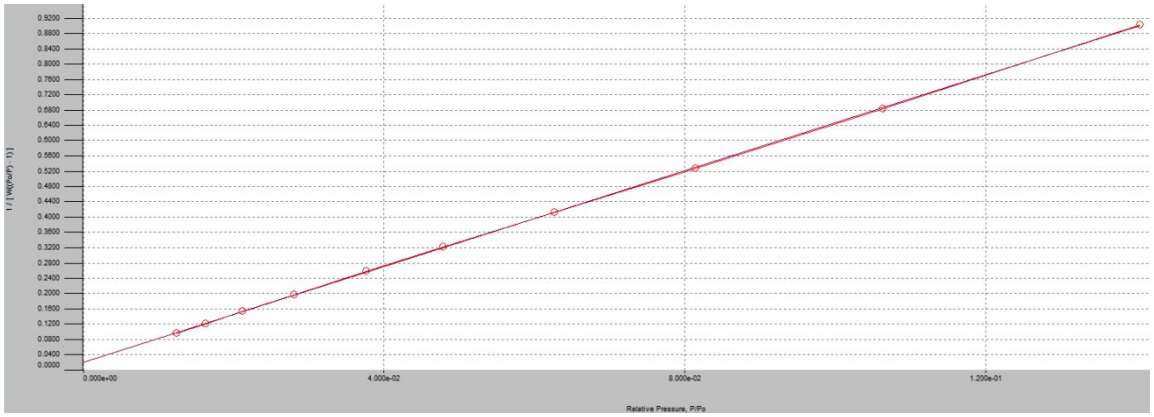

Figure S15. BET plots of CPOP (r = 0.999977, C = 325.499)

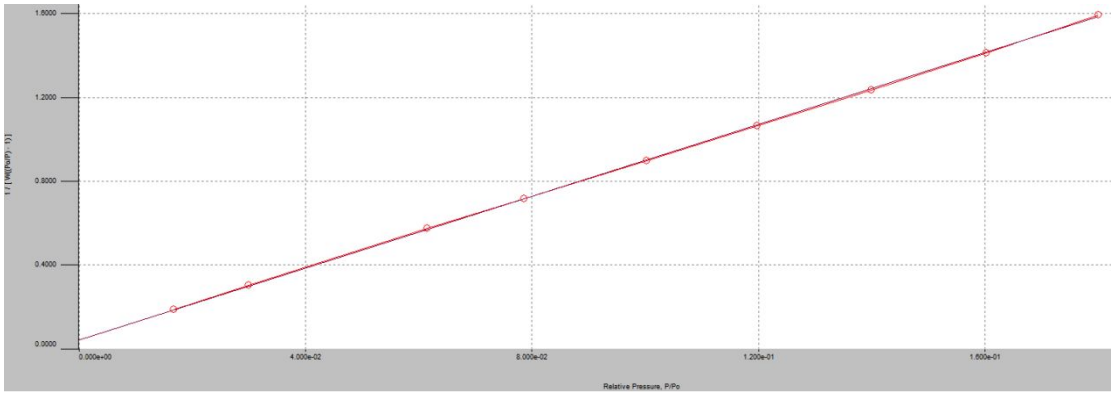

Figure S16. BET plots of AIPOP-1 (r = 0.999968, C = 199.189)

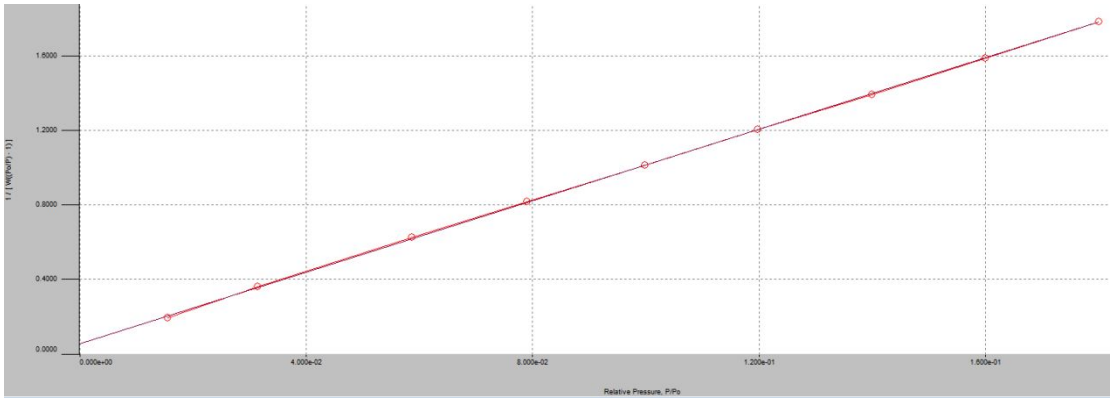

Figure S17. BET plots of AIPOP-2 (r = 0.999962, C = 172.029)

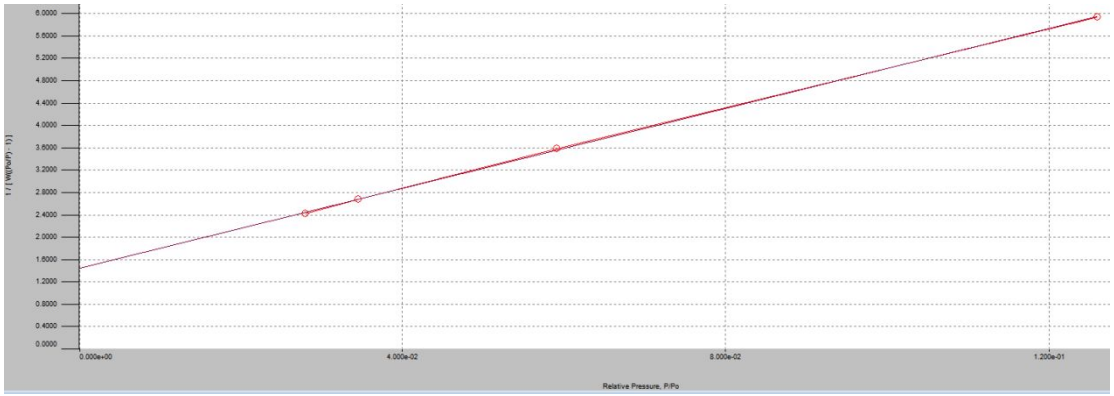

Figure S18. BET plots of AIPOP-3 (r = 0.999924, C = 25.726)

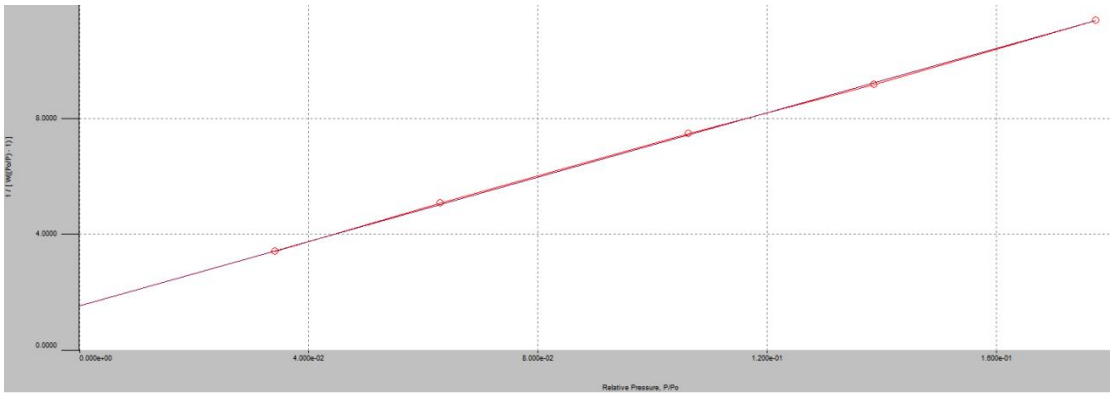

Figure S19. BET plots of AIPOP-4 (r = 0.999908, C = 36.885)

Table S1. Experimental data of AIPOPs and CPOP

Polymers	M-1 (mol)	M-2 (mol)	M-3 (mol)	C (%)	H (%)	N (%)	S_{BET} ($m^2\ g^{-1}$)	V_{total} ($cm^3\ g^{-1}$)	Iodine uptake ($g\ g^{-1}$)	Yield (%)
AIPOP-1	1	2	0.8	73.6	4.69	1.38	405	1.21	1.73	75.4
AIPOP-2	1	2	2.0	73.7	5.36	3.72	361	1.07	2.65	73.3
AIPOP-3	1	2	2.8	74.8	5.70	4.57	97	0.51	3.25	72.8
AIPOP-4	1	2	4.0	74.2	6.00	5.75	61	0.42	4.10	88

CPOP	1	2	0	75.4	4.41	0	554	2.44	1.15	85

Table S2. EDS analysis data for CPOP and AIPOP-1 to AIPOP-4

	C		N		Si		P	
	Mass (%)	Atom (%)	Mass (%)	Atom (%)	Mass (%)	Atom (%)	Mass (%)	Atom (%)
AIPOP-4	63.74	82.14	5.73	4.64	21.97	12.11	0.82	0.41
AIPOP-3	76.19	88.81	3.43	3.43	13.19	6.58	3.71	0.49
AIPOP-2	77.98	90.03	2.85	2.83	12.06	5.96	0.85	0.38
AIPOP-1	66.36	84.42	1.11	1.21	23.42	12.74	0.92	0.45
CPOP	61.89	97.63	-	-	9.81	5.94	1.14	0.62
	Br		Pd		Cs		Cu	
	Mass (%)	Atom (%)	Mass (%)	Atom (%)	Mass (%)	Atom (%)	Mass (%)	Atom (%)
AIPOP-4	1.06	0.2	4.51	0.66	3.17	0.37	-	-
AIPOP-3	0.69	0.12	3.71	0.49	1.97	0.21	-	-
AIPOP-2	1.56	0.27	1.57	0.2	3.14	0.33	-	-
AIPOP-1	0.58	0.11	6.78	0.97	0.83	0.1	-	-
CPOP	22.81	4.85	1.95	0.31	-	-	2.41	0.65

Table S3. Porosity data of CPOP and AIPOP-1~AIPOP-4.

Polymers	S_{BET} (m^2g^{-1}) [a]	S_{micro} (m^2 g^{-1}) [b]	V_{total} (cm^3 g^{-1}) [c]	V_{micro} (cm^3 g^{-1}) [d]	V_{micro}/V_{total}
CPOP	554	360.1	2.44	0.146	0.060
AIPOP-1	405	190.3	1.21	0.069	0.057
AIPOP-2	361	130.1	1.07	0.040	0.037
AIPOP-3	97	0	0.51	0	0
AIPOP-4	61	0	0.42	0	0

[a] Surface area calculated from N_2 adsorption isotherm using the BET method; [b] Microporous surface area calculated from N_2 adsorption isotherm using t-plot method;[c] Total pore volume calculated at P/P_0 = 0.99; [d] Micropore volume derived using the t-plot method based on the de-Boer thickness equation.

Table S4. Kinetic parameters for the I_2 adsorption by AIPOP-4

Model	Parameters	
	Q_{exp} (g g^{-1})	4.1

Pseudo-first order	$Q_{e,cal}$ (g g^{-1})	2.621
	K_1 (g g^{-1} h^{-1})	0.25543
	R^2	0.9718
Pseudo-second order	$Q_{e,cal}$ (g g^{-1})	4.162
	K_2 (h^{-1})	0.2329
	R^2	0.9941

Table S5. Kinetic parameters for the I_2 adsorption in *n*-hexane solution by AIPOP-4

Modal	Parameters	
Pseudo-first order	$Q_{e, cal}$ (g g^{-1})	0.24734
	K_1 (g g^{-1} h^{-1})	0.04712
	R^2	0.98157
Pseudo-second order	$Q_{e, cal}$ (g g^{-1})	0.2922
	K_2 (h^{-1})	0.968
	R^2	0.99102

Table S6. Summary of the Langmuir and Freundlich isotherm model parameters for the adsorption of iodine in *n*-hexane solution on the AIPOP-4

Langmuir constants			Freundlich constants		
Q_m(g g^{-1})	K_L(L g^{-1})	R_L^2	K_F(L g^{-1})	1/n	R_F^2
0.7874	1.72	0.9810	3.873×10^4	0.37	0.9924

Table S7. Electronic binding energy of various elements in iodine-loaded CPOP and AIPOP-4

Sample	$I3p_1$	$I3p_3$	$I3d_3$	$I3d_5$	N1s	C1s	
AIPOP-4	-	875.17	631.81	620.36	399.55	284.80	
CPOP	932.50	875.67	631.52	620.02	399.81	284.80	
	Br3s	$Br3p_1$	$Br3p_3$	Si2s	Si2p	Br3d	I4d
AIPOP-4	-	-	-	152.98	101.81	-	50.28
CPOP	257.63	190.93	183.79	153.29	102.17	70.91	51.14